# Comparison of Some Butadiene-Based Impact Modifiers for Polycarbonate

C. CHENG,[1] N. PEDUTO,[1] A. HILTNER,[1,*] E. BAER,[1] P. R. SOSKEY,[2] and S. G. MYLONAKIS[2]

[1] Department of Macromolecular Science, and Center for Applied Polymer Research, Case Western Reserve University, Cleveland, Ohio 44106; [2] EniChem America Inc., 2000 Cornwall Rd., Monmouth Junction, New Jersey 08852

SYNOPSIS

The relationship of blend morphology to deformation mechanisms and notched Izod impact strength was studied with three butadiene-based impact modifiers for polycarbonate (PC). The impact modifiers were a linear polybutadiene (PB), a styrene–butadiene–styrene block copolymer (SBS), and a structured latex particle having a PB core and methyl methacrylate/styrene shell (MBS). The particle-size distribution in the blends was determined from transmission electron micrographs (TEM). Fractographic analysis combined with TEM examination of thin sections from impacted specimens provided insight into the failure mechanisms. Good impact was achieved with PC/MBS blends when cavitation of the core–shell particles relieved triaxiality and enabled the matrix to fracture by the plane stress ductile tearing mode that is characteristic of thin PC. The best impact properties were obtained with PC/SBS blends when the modifier was dispersed as aggregates of small particles. Cavitation at the weak internal boundaries relieved triaxiality, but subsequent coalescence of cavitated particles during ductile drawing of the matrix created critical size voids and the resulting secondary cracks reduced the toughness of the blend. In general, PB did not significantly enhance the impact strength of PC. 

## INTRODUCTION

Polycarbonate (PC) is an engineering thermoplastic with excellent clarity, high heat-deflection temperature, and toughness in thin sections. However, its notched impact properties become poorer as the thickness increases. This notch sensitivity is due to the change in stress state at the notch from plane stress to plane strain and the resulting change in failure mechanism from shearing to crazing. The notch sensitivity can be reduced by blending a small amount of an elastomer with PC. Cavitation of the elastomer relieves the triaxiality at the notch and permits the matrix to deform by ductile shearing. The effectiveness of the elastomer in this function depends on various factors; the ones of particular interest in this study are the chemical architecture of the elastomer and the dispersion of the elastomer in the matrix.[1]

Linear polybutadiene (PB) alone is not commonly used for toughening ductile matrices. Without cross-linking, it has poor strength, and being difficult to disperse, the morphology of its blends is difficult to control. Instead, PB is incorporated as a component into copolymers or terpolymers of various architectures such as styrene–butadiene–styrene block copolymer (SBS) and structured latex particles with methyl methacrylate/styrene (MBS).

Styrenic block copolymers with high elastomer content possess a phase-separated morphology in which polystyrene (PS) domains function as physical cross-links for the continuous PB phase. These copolymers are quite attractive as impact modifiers because they significantly improve the toughness at relatively low cost.[2,3] Nevertheless, elastomer dispersion depends on the processing conditions, so these must be optimized if the best properties are to be achieved.

The core–shell elastomers are designed specifically to produce blends with good dispersion and toughness under a wide range of processing condi-

* To whom correspondence should be addressed.

Journal of Applied Polymer Science, Vol. 53, 513–525 (1994)
 CCC 0021-8995/94/050513-13

tions. Size and uniformity of the structured latex particles are predetermined. The lightly cross-linked PB core determines the cavitation resistance of the particle, whereas the shell provides rigidity so that the particles retain their spherical shape during processing. The chemical composition of the shell is also chosen to impart compatibility with the matrix for ease of dispersion during processing and good adhesion subsequently.[4]

Optimization of the extrusion parameters for mixing these blends was the subject of a previous statistically designed experimental study.[1] The effects of screw design and operating parameters on the resultant impact strength were discussed. The present morphological investigation of selected specimens from the previous study was undertaken to examine more closely the relationship of particle size and distribution to deformation mechanisms and notched impact strength.

## EXPERIMENTAL

The matrix material was a bisphenol-A type polycarbonate (PC) (Sinvet 251, EniChem). The three elastomeric modifiers were a linear polybutadiene (PB) (Intene 40A, EniChem), which is a low *cis* content (40%) rubber typically used in the manufacture of HIPS and ABS; a linear sytrene–butadiene–styrene block copolymer (SBS) (Europrene TE-6302, EniChem) with 70% by weight butadiene; and a structured latex having a PB core and a methyl methacrylate/styrene shell (MBS) (Paraloid EXL-3607, Rohm and Haas). The GPC molecular weights and viscosities are given in Table I.

Blending of the elastomers (5 wt%) and PC was described previously.[1] Compounding was performed on a Leistritz co-rotating intermeshing 34 mm twin-screw extruder with three screw designs: (1) kneading disk (KD) consisted of forwarding screw elements followed by sections of kneading disks—the kneading disks provided high shear that enhanced dispersive mixing; (2) back flow (BF) consisted of the forwarding elements with a reverse screw section—the back flow aided distributive mixing; and (3) kneading disk and back flow (KD + BF), where both elements were included to provide dispersive and distributive mixing.

Impact specimens were produced with a 28 ton Engel injection-molding machine. A Tinius Olsen pendulum impact testing machine with a low-temperature unit and an instrumented tup was used to perform all the impact tests. Notched Izod specimens 6.35 mm thick were prepared and tested. The effects of processing characteristics and screw design on impact strength were discussed previously.[1] For the present study, specific impacted specimens were chosen for detailed analysis of morphology, failure mechanisms, and fracture. These specimens are identified by the elastomer abbreviation (MBS, SBS, PB), followed by a number that is the impact strength in units of J/m.

Optical and electron microscopy were used to examine the morphology of undeformed specimens. Injection-molded specimens were precracked and broken at liquid nitrogen temperature. The cryogenic fracture surfaces were coated with a thin layer of Au/Pd and examined in a JEOL 840A scanning electron microscope (SEM). To enhance particle contrast for optical microscopy, undeformed specimens were stained in a 2% aqueous solution of osmium tetroxide for 3 days, then microtomed with a glass knife. The microtomed surfaces were examined with an Olympus BH optical microscope (OM) in the reflection mode. Sections for transmission electron microscopy (TEM) were prepared by embedding the specimen in epoxy, followed by trimming and staining for 3 days in a 2% aqueous solution of osmium tetroxide. Sections were then microtomed at room temperature with an RMC MT6000-XL ultramicrotome. The 80–110 nm-thick sections were examined in a JEOL 100SX transmission electron microscope.

Particle-size distributions were obtained with the aid of an Olympus Cue-4 image analysis system. Micrographs were scanned by a high-resolution charge-coupled device camera (500 × 582 pixels) and the image was transmitted to the image monitor

**Table I Material Properties (from Ref. 1)**

| Materials | $M_n$ | $M_w$ | $M_w/M_n$ | $\eta^a$ (Pa-s) |
|---|---|---|---|---|
| PC–Sinvet 251 | 17,000 | 30,000 | 1.8 | 1200 |
| PB–Intene 40A | 124,000 | 283,000 | 2.3 | 1000 |
| SBS–Europrene TE-6302 | 100,000 | 142,000 | 1.4 | 800 |

[a] Measured at 250°C and shear rate of 1000 $s^{-1}$.

and analyzed on a personal computer. All particle-size histograms were constructed from analysis of 500 or more particles.

The fracture surfaces of Izod-impacted specimens were examined by both OM and SEM. Longitudinal sections 0.2 mm thick were cut from the center region of the impacted specimens with a water-cooled diamond blade operated at a slow speed and the damage zone above and below the fracture surface was examined in the OM in the transmission mode. Thin sections were microtomed from the deformed region adjacent to the fracture surface following the procedures described for undeformed specimens. The deformed particles in these sections were examined in the TEM.

## RESULTS AND DISCUSSION

### Process History and Impact Strength

The parameter used to characterize the process history was the specific energy consumption (SEC) defined as the energy input to the compounding extruder per unit mass of material processed. The relationship between SEC and notched Izod impact strength of 6.35 mm-thick specimens is plotted in Figure 1 using data from the previous study.[1] The impact strength was highest for blends with the MBS core–shell rubber; furthermore, the impact strength of MBS blends at 25°C was insensitive to the processing conditions. The sample in Figure 1(a) that was injection-molded without prior compounding (SEC = 0) possessed the same impact strength as that of the compounded samples at this temperature. The impact strength of the compounded blends dropped from 800 J/m at 25°C to 400 J/m at −20°C. At this temperature, compounding before injection molding produced a higher impact strength than did injection molding only. The sample with SEC = 0 had an impact strength at −20°C of only about 150 J/m, which was no better than the unmodified PC.

The 25°C impact strength of blends with SBS was very sensitive to processing conditions, as shown in Figure 1(b). The lowest SEC produced the blend with the highest impact strength. An increase in SEC was initially accompanied by a rapid decrease in the impact strength from 606 to about 200 J/m, a value that was only slightly higher than the unmodified PC. As SEC increased further, the impact strength remained essentially unchanged from 200 J/m. The SBS blend that was injection-molded only without compounding demonstrated no improvement in impact strength over the unmodified PC. Unlike MBS, compounding was required to break up and disperse the bulk SBS elastomer as the micron-sized particles required for impact enhancement. It appeared, however, that SBS could easily be overcompounded with PC with the concomitant loss in impact strength.

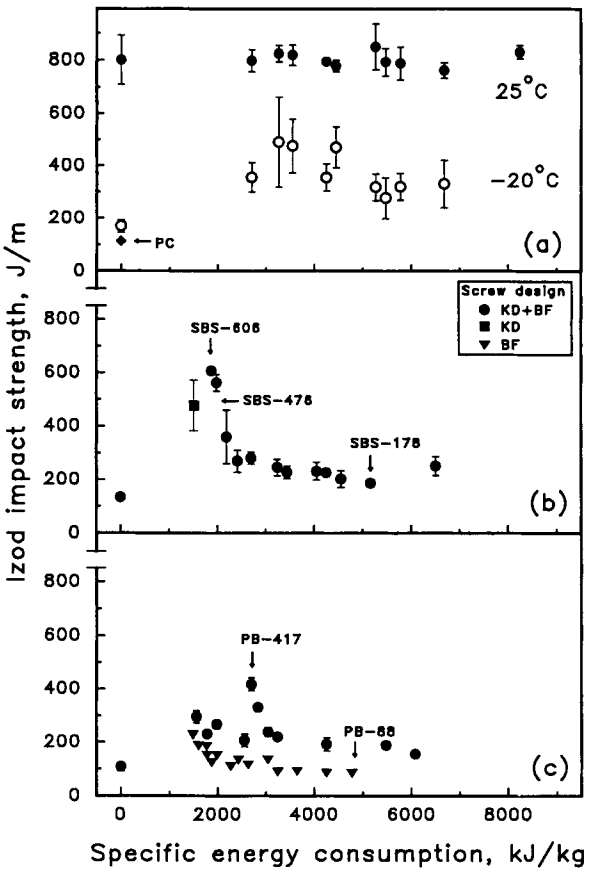


**Figure 1** Impact strength as a function of specific energy consumption (SEC) for PC blended with (a) MBS, (b) SBS, and (c) PB. Data from Ref. 1.

The PB rubber was much less effective as an impact modifier for PC than was either MBS or SBS [Fig. 1(c)]. There was no obvious relationship between impact strength and SEC for these blends, although perhaps a gradual decrease in impact strength from 300 to 150 J/m could be discerned. A couple of blends had impact strengths near 400 J/m; however, these were exceptions and it was difficult to control the processing to achieve this property value.

### Blends with MBS

Micrographs of the undeformed PC blends with MBS showed uniform, well-dispersed spherical par-

ticles about 0.2 μm in diameter [Fig. 2(a)]. In general, TEM micrographs also showed good dispersion of MBS particles in the uncompounded blend; only occasionally were regions with exceptionally high or low particle concentration encountered [Fig. 2(b) and (c)]. Although these regions did not affect the 25°C impact, they compromised the low-temperature impact strength of the blends.

Fractography is widely used in postfracture analysis of metals and other opaque materials to understand, from the appearance of the fracture surface, where the fracture originated, how it propagated, and whether it was ductile or brittle. Fracture surfaces of PC/MBS blends impacted at 25°C were ductile and completely stress-whitened. A representative fracture surface of the blend in Figure 3(a) shows tear lines with characteristic sucking-in of the edges, which is indicative of plane stress shear fracture. There was about a 19% decrease in thickness due to the sucking-in. The fractured specimen was sectioned longitudinally on the center plane; the resulting side view of the fracture in Figure 3(b) shows a stress-whitened zone that extended about 1.5 mm above and below the fracture plane. The zone was uniformly and intensely stress-whitened, and a sharp boundary differentiated the zone from the surrounding material.

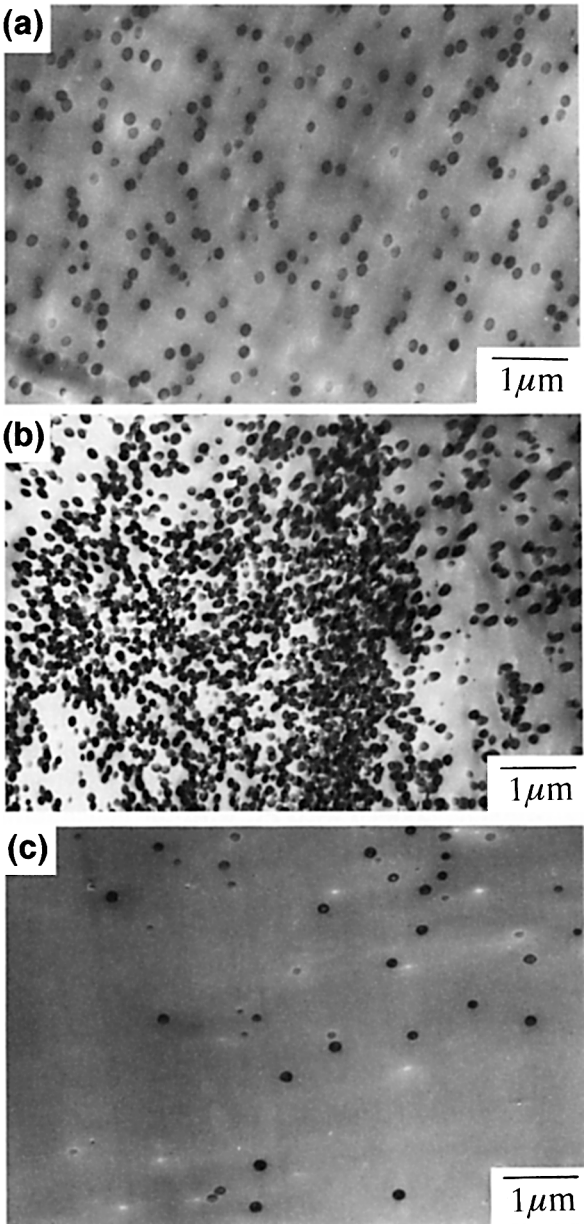


**Figure 2** TEM micrographs of undeformed PC/MBS blends: (a) compounded; (b, c) injection-molded without compounding.

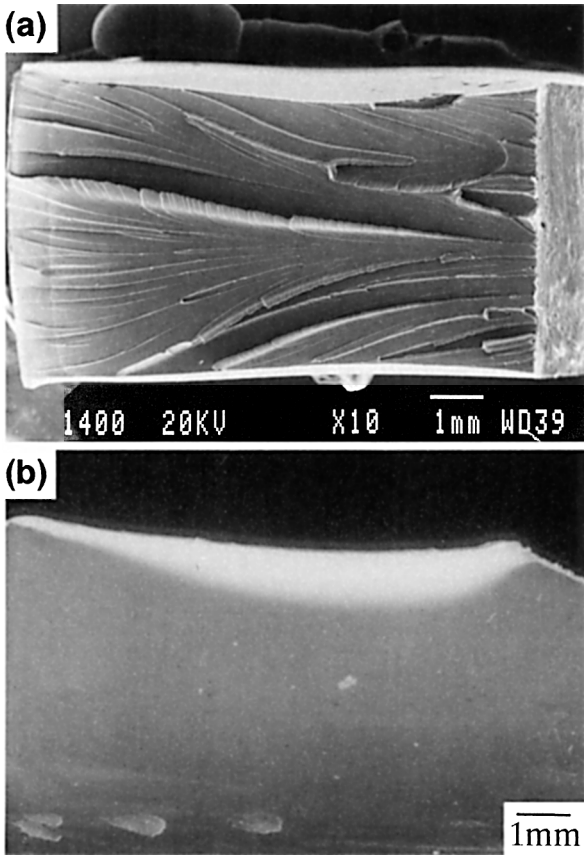


**Figure 3** Fracture surface of impacted PC/MBS blend: (a) top view (SEM); (b) side view (OM).

Deformation of the particles was visible in a higher magnification SEM micrograph of a region in the center of the fracture surface [Fig. 4(a)]. Cavitated particles appeared as randomly dispersed voids on the relatively smooth fracture surface. Light scattering by the numerous voided particles was re-

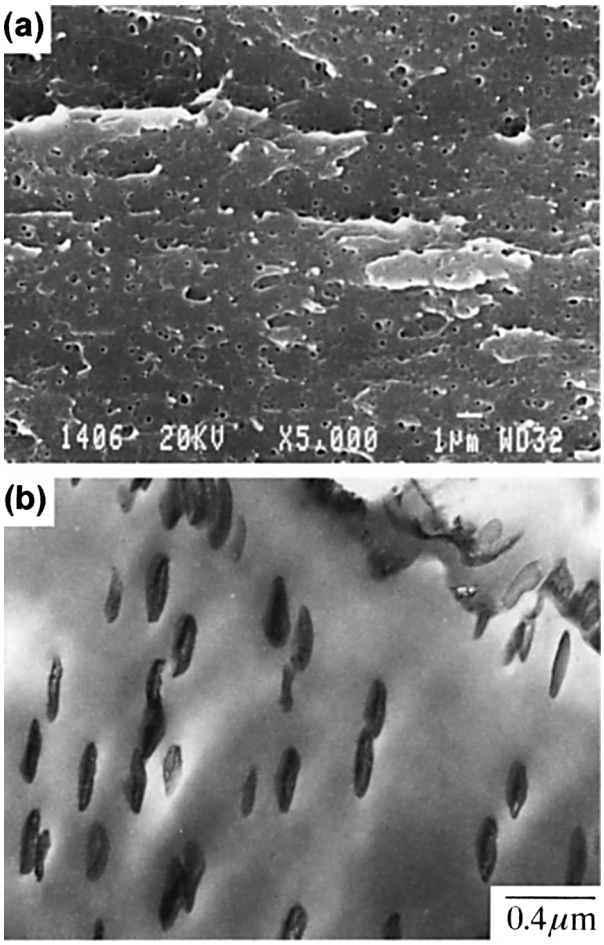


**Figure 4** Impacted PC/MBS: (a) high magnification of the fracture surface in Figure 3(a) (SEM); (b) a longitudinal section through the damage zone; the fracture surface is visible in the upper right corner (TEM).

sponsible for the stress whitening. The size and shape of the voided particles in the region immediately above or below the fracture surface is seen in the longitudinally microtomed section in Figure 4(b). The cavitated particles were highly elongated with a draw ratio in the range of 1.5–2.0, approximately the natural draw ratio of PC. The width of the cavitated particles was about 0.08 μm and corresponded to the diameter of the voids on the fracture surface. The cavitated particles were aligned at an angle of 25°–45° to the fracture plane. This incline, together with the elongated shape of the particles, indicated plane stress plastic tearing of the matrix during ductile crack propagation.[5]

Particle cavitation was a desirable deformation mechanism of the blend since it relieved the triaxiality, thereby enabling the PC to yield and draw. Plastic deformation of the matrix was the energy absorption mechanism primarily responsible for the high impact strength of PC blends. In the MBS blends, particle cavitation was not followed by coalescence of the voids, which could have had a detrimental effect if the coalescence had created critical-size flaws. Instead, cavitation of the MBS blends was followed by the plane stress ductile tearing mode of fracture that is characteristic of thin PC.

## Blends with SBS

### *Morphology*

Examination by SEM of fracture surfaces obtained when the PC/SBS blends were cryogenically fractured parallel and perpendicular to the injection direction revealed irregularly shaped rubber particles ranging in diameter from less than 1 micron to several microns. The morphology in the region close to the edge appeared to be the same as that in the center with no variation in particle size or shape through the thickness of the injection-molded pieces. In particular, there was no elongation of particles near the edge that would have indicated a skin–core morphology. The skin–core morphology is frequently observed in injection-molded PC blends with a relatively low viscosity ratio (dispersed phase/matrix), on the order of 0.1–0.3.[6,7] The absence of this feature in the PC/SBS blends was attributed to the high viscosity ratio of 0.66.

Particle-size distribution was characterized in the PC/SBS blends with the highest (SBS-606) and lowest (SBS-178) impact strengths. Transmission electron micrographs of sections taken from the center parallel to the injection direction in Figure 5 illustrate the large range in particle size and the irregular shape, especially of the larger particles. Furthermore, comparison of the two morphologies in Figure 5 showed that the SBS particles were larger in the blend with the highest impact strength.

The particle-size distribution was obtained by image analysis of 500 particles in randomly selected micrographs. No attempt was made to correct the particle size for the effect of section thickness. The Martin's radius, defined as the distance from the center of gravity to the edge of the particle, was measured at 45° intervals to obtain eight values. The particle size was taken as twice the mean Martin's radius, and the distributions are plotted in Figure 6 by both number fraction and volume fraction. The number fraction distribution in Figure 6(a) showed a maximum at 0.3 μm for both blends, but the distribution in the blend with the highest impact strength was broader and more skewed toward large particle sizes. The difference was more evident when

the contribution of large particles was emphasized by plotting the volume fraction [Fig. 6(b)]. In this plot, the distribution was more symmetrical, with the maxima at particle sizes of 1.1 $\mu$m for the low impact blend SBS-178 and at 1.6 $\mu$m for the high impact blend SBS-606.

Examination of the particle-size distribution in other PC/SBS blends confirmed the correlation between larger particles and better impact strength. This is illustrated in Figure 7, where impact strength is plotted as a function of both number-average and volume-average particle size. The SBS particle size was determined by process history. Blends with larger particles were those that were processed with lower SEC; higher SEC produced overmixed blends when the longer residence time in the extruder reduced the particle size sufficiently that impact enhancement was adversely affected.

### *Deformation*

The loss in toughness as the volume-average particle size decreased was reflected in the appearance of the fracture surfaces as illustrated in Figure 8, with PC/SBS blends having volume-average particle diameters of 1.76 $\mu$m (SBS-606), 1.63 $\mu$m (SBS-476), and 1.19 $\mu$m (SBS-178). The ductile fracture surface of SBS-606 was completely stress-whitened with a 13% decrease in thickness due to sucking-in. Markings characteristic of herringbone fracture were

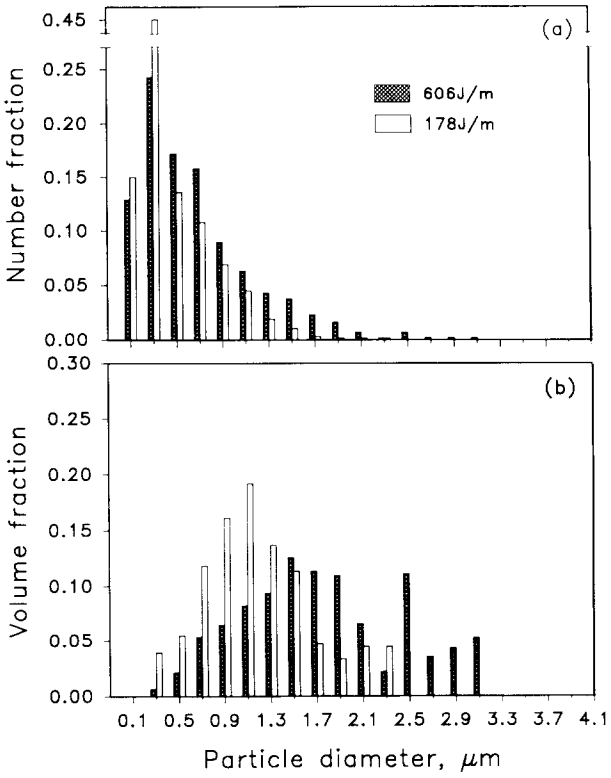


**Figure 6** Number fraction and volume fraction particle-size distributions of SBS-606 and SBS-178 from TEM micrographs.

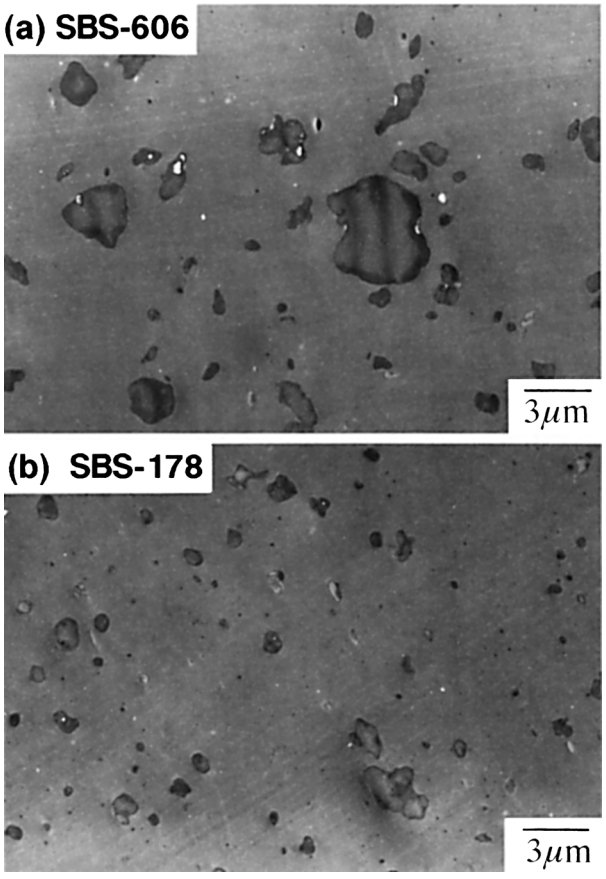


**Figure 5** TEM micrographs of undeformed PC/SBS blends: (a) SBS-606; (b) SBS-178.

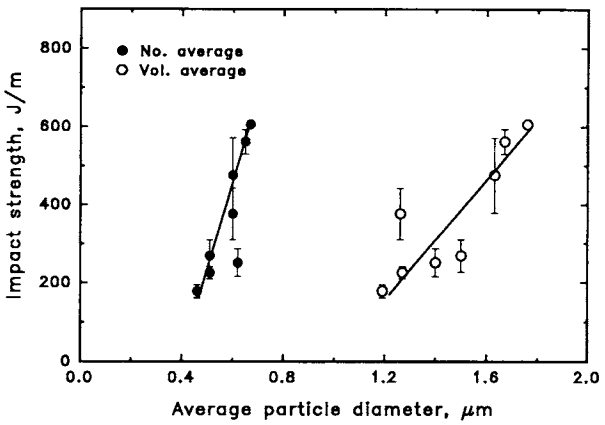


**Figure 7** Impact strength of PC/SBS blends as a function of number-average and volume-average particle size.

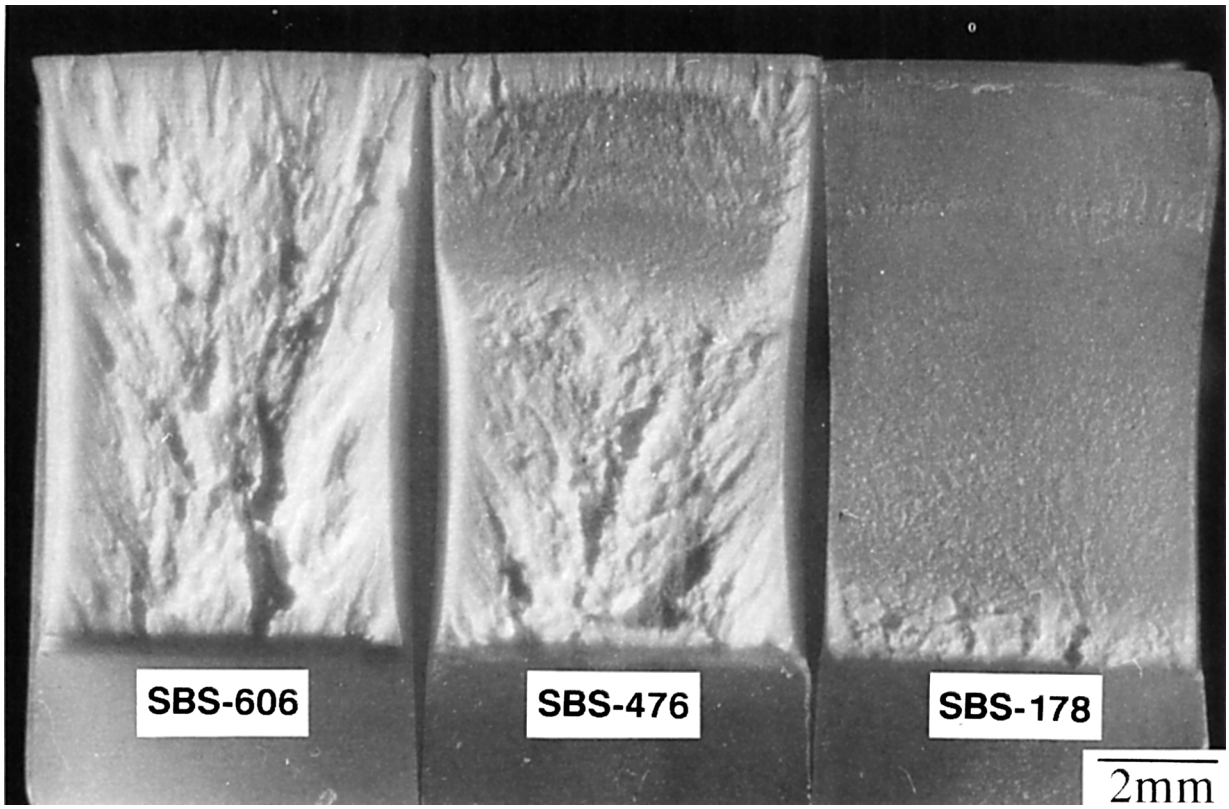


**Figure 8** Fracture surfaces of impacted PC/SBS blends (OM).

identifiable on the fracture surface. The fracture surface of SBS-476 consisted of a stress-whitened ductile region that started at the notch root and extended to a brittle region further from the notch. The fracture surface of SBS-178 possessed only a small region of stress whitening at the notch root; otherwise, the surface was featureless and brittle. In general, there was a linear relationship between the area of stress whitening on the fracture surface and the Izod impact strength of PC/SBS blends.

A side view through the center of the fracture showed a damage zone composed of two regions: a zone of intense stress whitening adjacent to the fracture plane and a larger region of more diffuse stress whitening extending some distance from the fracture plane [Fig. 9(a) and (b)]. The zones were not differentiated by sharp boundaries. When viewed under crossed polars, only the intense zone exhibited birefringence from plastic deformation of the matrix [Fig. 9(c)]. Most of the impact energy was absorbed in the intense zone where profuse voiding was accompanied by plastic deformation; voiding also characterized the diffuse zone further from the fracture surface, but without plastic deformation of the matrix, the contribution of this region to the impact strength was much smaller.

A TEM micrograph of a section microtomed from the intense zone directly beneath the fracture surface is shown in Figure 10. Most of the SBS particles were cavitated, as indicated by the remnants of rubber adhered to the sides of the cavities. The cavitated particles were somewhat elongated but the particle draw ratio was considerably less than the natural draw ratio of PC. Furthermore, the elongated particles were aligned 90° to the fracture surface rather than at an inclined angle that would have indicated ductile tearing fracture. It was concluded that the blend fractured before the matrix was fully drawn out. Some of the voids in the intense zone were as large as 8 $\mu$m in diameter, about twice the diameter of the largest particles. These may have resulted from coalescence of two or more cavitated particles. If the voided particles were close together, the PC ligament separating them could easily have fractured when it was drawn out during plastic deformation. The diffuse zone was characterized by fewer cavitated particles and those that were cavitated formed smaller voids when compared with the intense zone.

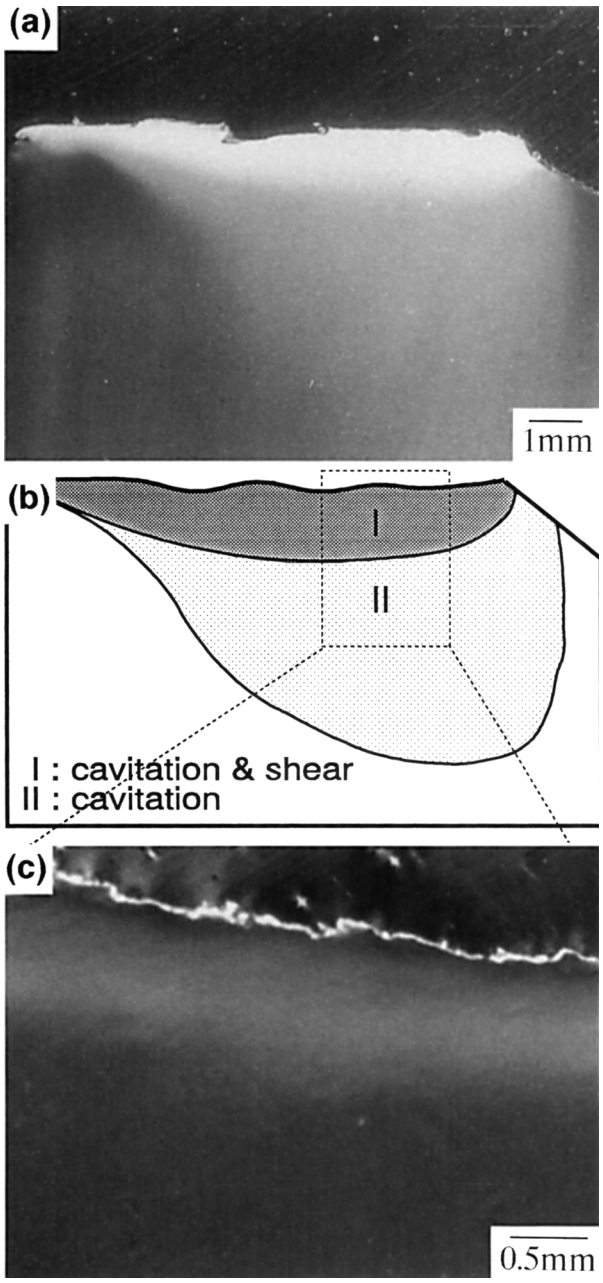


**Figure 9** Side view of the fracture surface of SBS-606: (a) bright field (OM); (b) sketch of the damage zone; (c) crossed polars (OM).

Coalescence of the voids was not observed in this region.

It appeared from the micrographs that all the uncavitated particles in the intense stress-whitened zone were small particles. This impression was confirmed by comparing the particle-size distribution of uncavitated particles in the intense zone of the impacted blend SBS-606 with the original particle-size distribution in the undeformed blend. Analysis of 350 uncavitated particles produced the distribution in Figure 11, which differed significantly from the original distribution by including only small particles with no particles larger than about 1 $\mu$m. From this result, it would be anticipated that SBS blends with a preponderance of small particles would have poor impact properties since most of the rubber particles would not cavitate and therefore would not contribute to relief of the hydrostatic strain energy.

Based on interparticle distance concepts, it is generally thought that rubber toughening of ductile thermoplastics is enhanced as the particles are made smaller, to a limit of about 0.2 $\mu$m.[8-10] Even in the PC/SBS blends with the smallest particles, most of the particles were larger than 0.2 $\mu$m. Nevertheless,

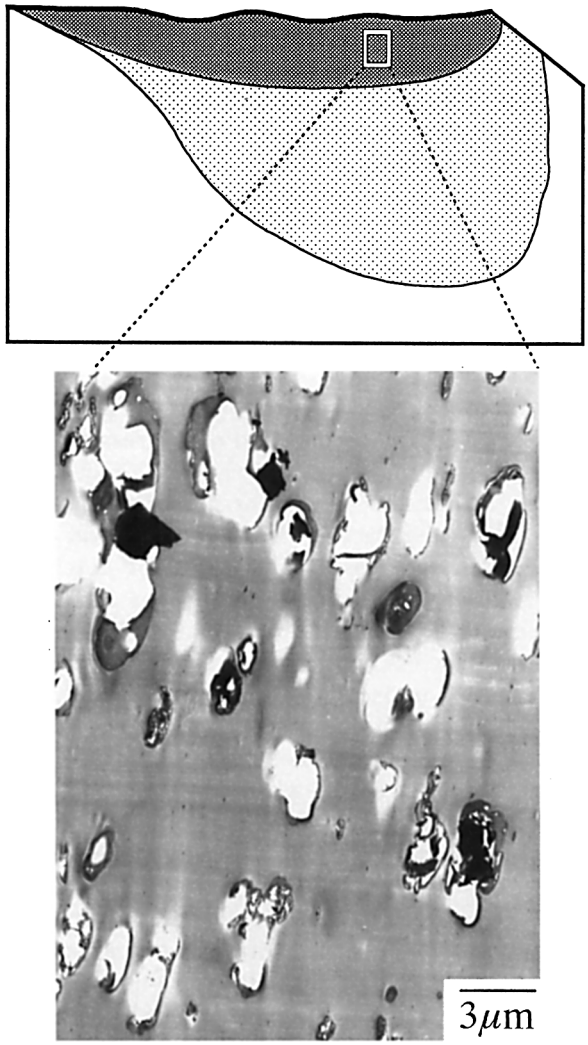


**Figure 10** A longitudinal section through the zone of intense stress whitening close to the fracture surface of SBS-606 (TEM).

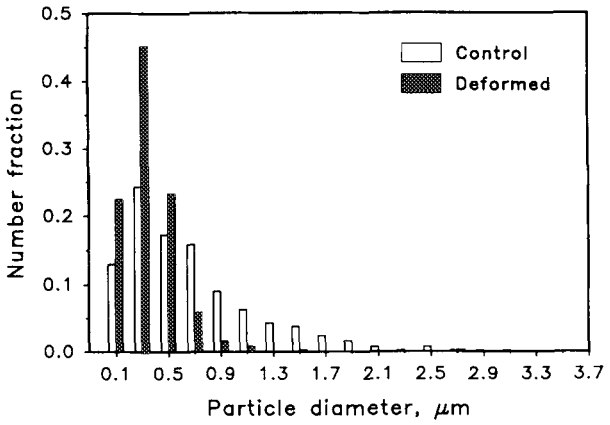


**Figure 11** Comparison of number fraction particle-size distributions of all particles in the undeformed blend with uncavitated particles in the intense stress-whitening zone of the impacted blend, SBS-606.

these blends exhibited the reverse trend in the relationship between particle size and impact strength. The reason for the high cavitation resistence of the small particles was sought in the particle morphology. With 70% by weight PB in the SBS, the domain morphology of this triblock copolymer was a combination of cylinders and lamellae as shown in the high-magnification transmission electron micrographs in Figure 12. Whereas the domain morphology extended through the small particles [Fig. 12(a)], the large particles appeared to be aggregates of smaller particles separated by "grain boundaries" [Fig. 12(b)]. Cavitation of the large particles initiated along these weak internal boundaries [Fig. 12(c)]. Since the boundaries were not present in the small particles, cavitation would have had to initiate within the domain structure where the cavitation resistence was much higher.

### *Fracture*

A low-magnification SEM micrograph of the entire fracture surface of the PC/SBS blend with the highest impact strength in Figure 13(a) shows the characteristic texture of a herringbone fracture.[11] A herringbone fracture is a plane strain fracture mode and is considered a brittle fracture mode of metals. However, when it is observed in polymer blends, such as in PC/ABS as well as in the PC/SBS blends in this study, it is associated with ductile fracture. The herringbone pattern consists of a center region and an edge region with a series of ridges that curve outward from the center. The identifing markings are produced when the main crack repeatedly interacts with secondary cracks that initiate along the centerline.

The parabolic markings in the center region of the PC/SBS herringbone pattern were a manifestation of secondary crack initiation. The parabolic

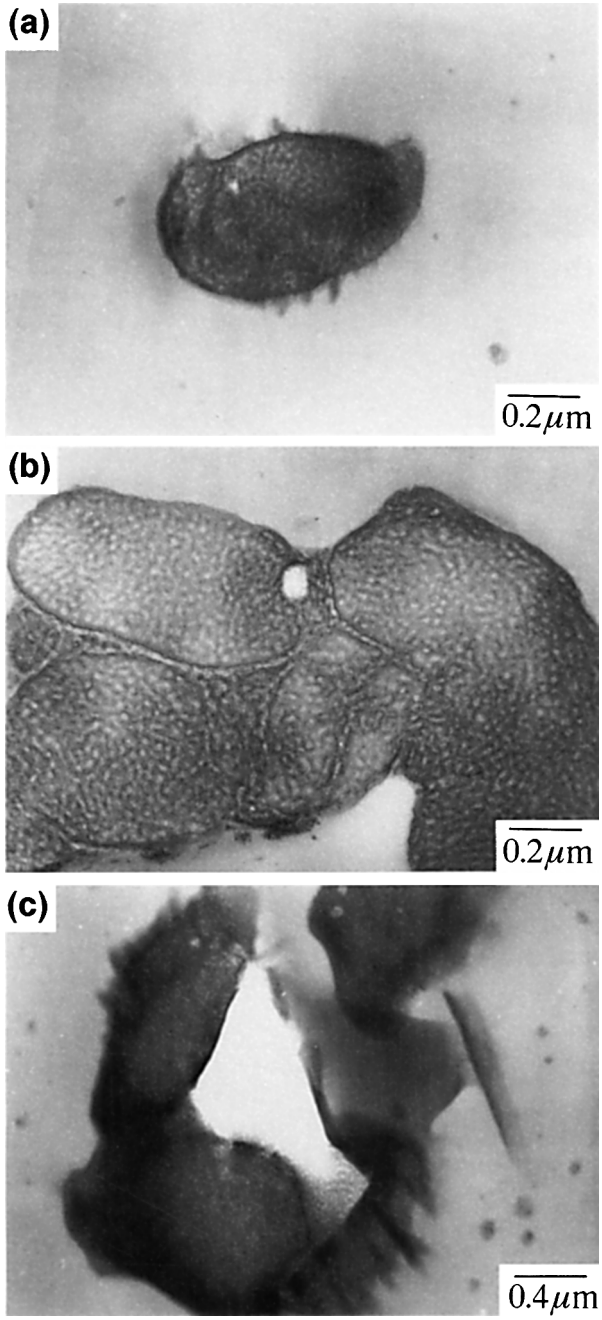


**Figure 12** High-magnification TEM micrographs of SBS particles: (a) small particle with no internal boundaries; (b) larger aggregate particle with internal boundaries; (c) deformed particle with cavitation at the internal boundaries.

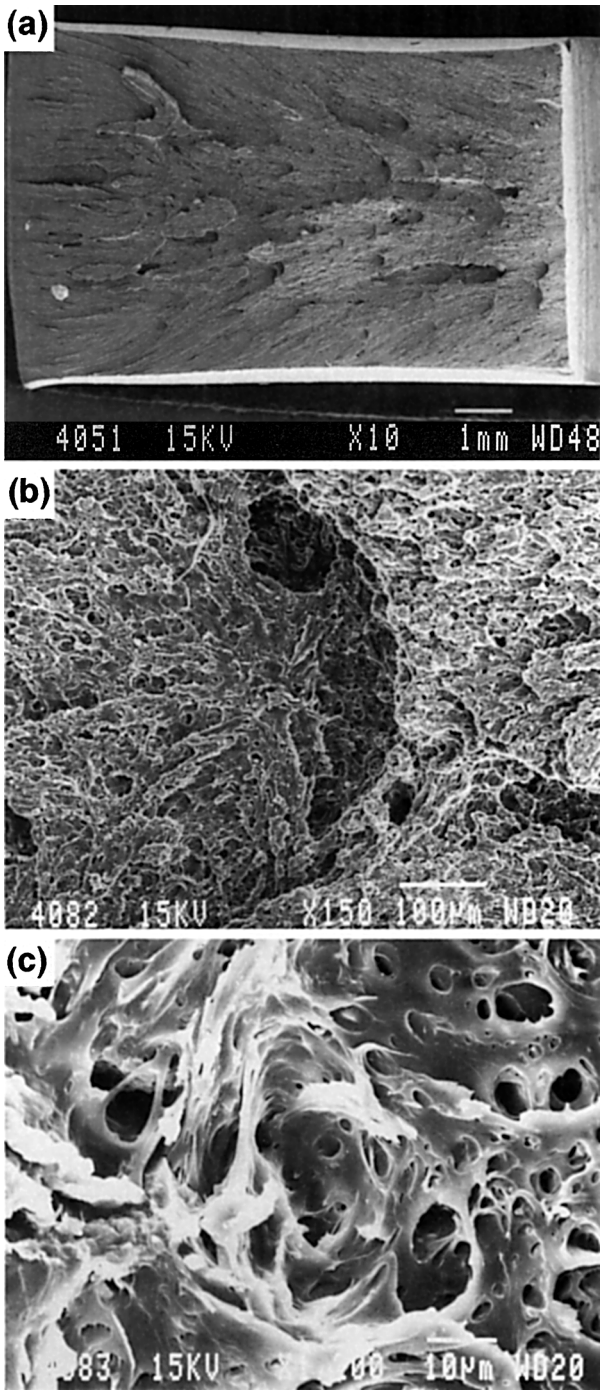


**Figure 13** Fracture surface of impacted SBS-606 (SEM): (a) low magnification of the entire surface; (b) higher magnification of a parabolic arc; (c) initiation site of the parabolic mark.

arc was produced by impingment of the primary crack front on a secondary crack front that initiated at a site near the parabolic arc. Since the parabolic marking was produced by the interaction of a single secondary crack with the primary crack, it was possible to locate the secondary crack initiation site and determine its source. A higher magnification of one of these markings in Figure 13(b) shows the parabolic arc with the initiation site of the secondary crack. An even higher magnification of the initiation site in Figure 13(c) shows that it was created by coalesced voids. The crack initiated when enough cavitated rubber particles had coalesced to create a critical-size flaw. In this example, the initiation site measured about 30 $\mu$m. Secondary crack initiation was confined primarily to the center region where the higher hydrostatic stress promoted cavitation and subsequent coalescence.

Particle cavitation was a key element in the impact enhancement of PC since it relieved the triaxiality, thus enabling the ductile matrix to draw. However, coalescence of the voided particles had a detrimental effect on toughening when the coalesced voids reached a critical size for secondary crack initiation. It was demonstrated that the large SBS particles cavitated easily to relieve triaxiality; however, both TEM sections and the fracture surfaces provided evidence that the voids subsequently coalesced as the matrix was drawn out. Secondary crack initiation from the coalesced voids facilitated crack propagation, and as a result, fracture occurred before the matrix was fully drawn out.

## Blends with PB

### *Morphology*

Optical micrographs of sections taken from the center region parallel to the injection direction in Figure 14 compare the morphology of PC/PB blends with the highest (PB-417) and lowest (PB-88) impact strengths. The PB particles in the blend with better impact strength were small and uniformly dispersed, whereas a large variation in particle size was seen in the blend with the poorest impact, including some very large particles that measured tens of microns in diameter. Comparison of particle size and shape in sections from the center and near the edge revealed no evidence of morphology variations through the thickness of the injection moldings. As with the PC/SBS blends, the close viscosity ratio of PC and PB, 0.83, was responsible for the absence of a skin–core morphology.

The TEM micrographs in Figure 15 show the blend morphology at higher magnification. The uniformly dispersed particles of the highest-impact blend were about 1 $\mu$m in diameter, whereas the lowest impact blend again had a wider range of par-

ticle sizes and shapes with particle diameters of 0.1–5 μm. This blend also contained even larger particles that did not appear in the small sections examined in the TEM.

Because of the extremely broad distribution of particle sizes in the PC/PB blends, from 0.1 to 100 μm, it was necessary to use both OM and TEM to obtain an accurate description of the size distribution. Particles in the size range from 0.1 to 7 μm were analyzed in the TEM micrographs. The volume fraction distribution of particle sizes determined from TEM only is shown by the open bars in Figure 16. Optical microscopy was used to analyze particles larger than 0.5 μm, and the results from TEM and OM were combined by normalizing the distributions to the area analyzed. The combined distribution is shown by the shaded bars in Figure 16. The volume fraction was plotted to emphasize the contribution of the large particles, and the bars for sizes larger than 15 μm usually indicated a single particle. Although one or two large particles could easily skew the distribution, it was significant that about 50% of the rubber in the highest-impact blend was dispersed as small particles in the 2 μm range, whereas less than 5% of the rubber in the poorest-impact blend was present as particles with diameters of 5 μm or less.

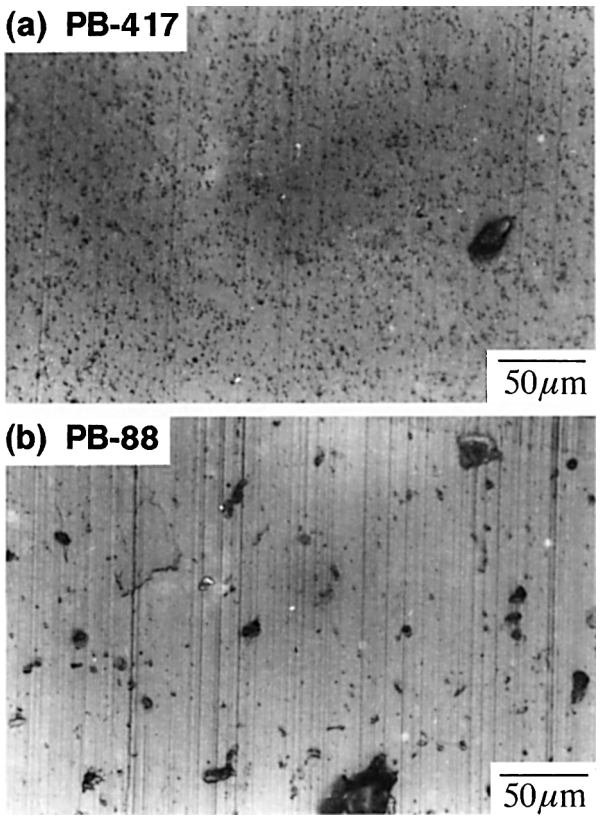


**Figure 14** OM micrographs of undeformed PC/PB blends: (a) PB-417; (b) PB-88.

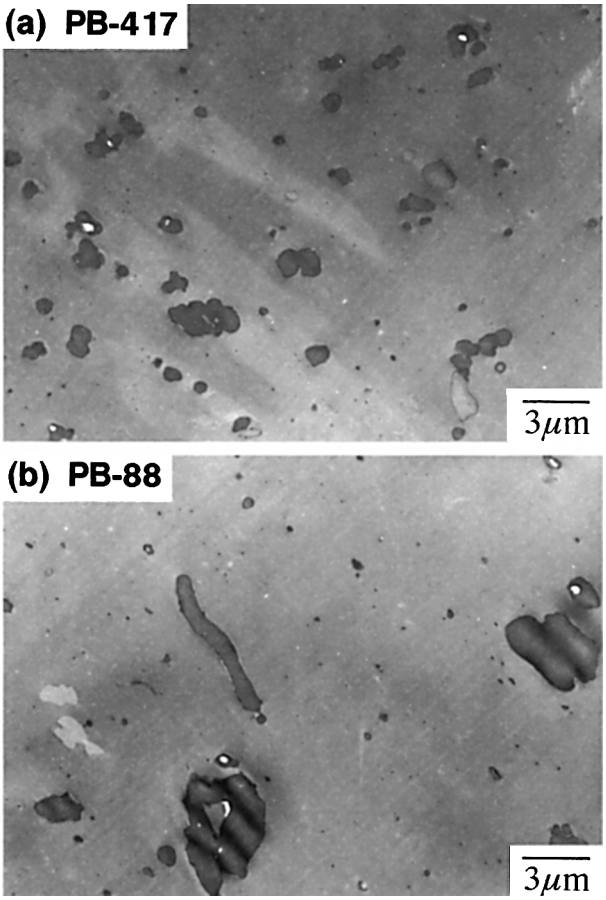


**Figure 15** TEM micrographs of undeformed PC/PB blends: (a) PB-417; (b) PB-88.

### *Fracture*

The low-magnification SEM micrograph in Figure 17(a) shows the fracture surface of the PC/PB blend with the highest impact strength. A ductile fracture mode was indicated by complete stress whitening of the surface and sucking-in with about an 11% reduction in thickness. The fracture markings resembled the herringbone to some extent: profuse secondary cracking in the center region produced islandlike features. As the triaxiality decreased toward the edges, the secondary cracks became less numerous and parabolic markings were observed. Finally, at the edges, ridges that curved outward were created by interaction of growing cracks. Compared to the PC/MBS and PC/SBS

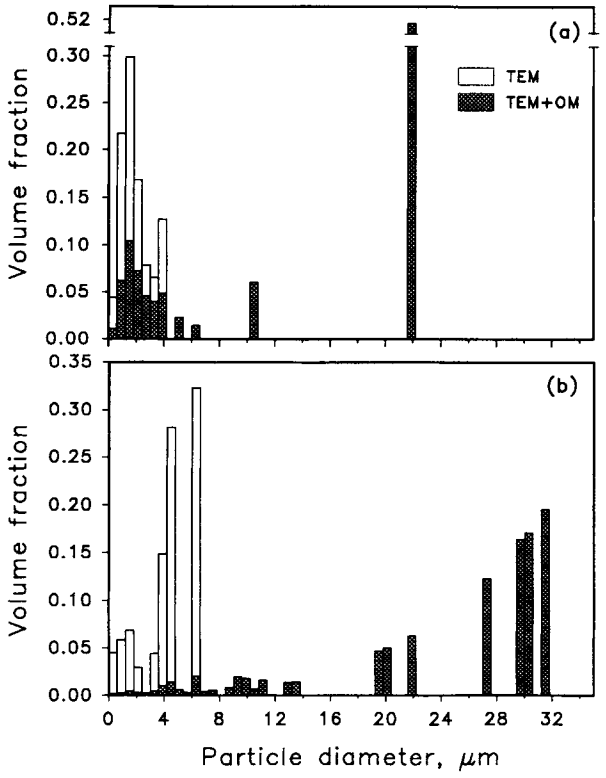


**Figure 16** Volume fraction particle-size distributions of PC/PB blends: (a) PB-417; (b) PB-88.

blends, the rougher texture on the fracture surface of the PC/PB blend and the lesser amount of sucking-in were consistent with the lower impact strength.

A higher magnification of the fracture surface showed undeformed rubber particles at the base of large cavities [Fig. 17(b)]. The debonded particles were typically 15 μm or larger in diameter. The cavities created by the debonding were in the range of 20–40 μm, depending upon the size of the rubber particle and the extent to which the matrix had deformed around the debonded particle. Little or no plastic deformation of the matrix was visible at debonded particles on the fracture surfaces of the most brittle PC/PB blends. Other voids were observed on the fracture surface that did not contain rubber particles. These empty voids could have resulted from debonding when the rubber particle remained on the matching fracture surface; alternatively, rubber particles might have cavitated and coalesced to create voids that appeared to contain no rubber. A TEM micrograph of a section microtomed longitudinally through the center region of the fracture surface in Figure 17(c) shows cavitation, rather than debonding, of the smaller rubber particles. The micrograph also contains the cross section of a large void on the fracture surface (upper left corner) that was created by coalescence of the cavitated particles.

Both debonding of large particles and coalescence

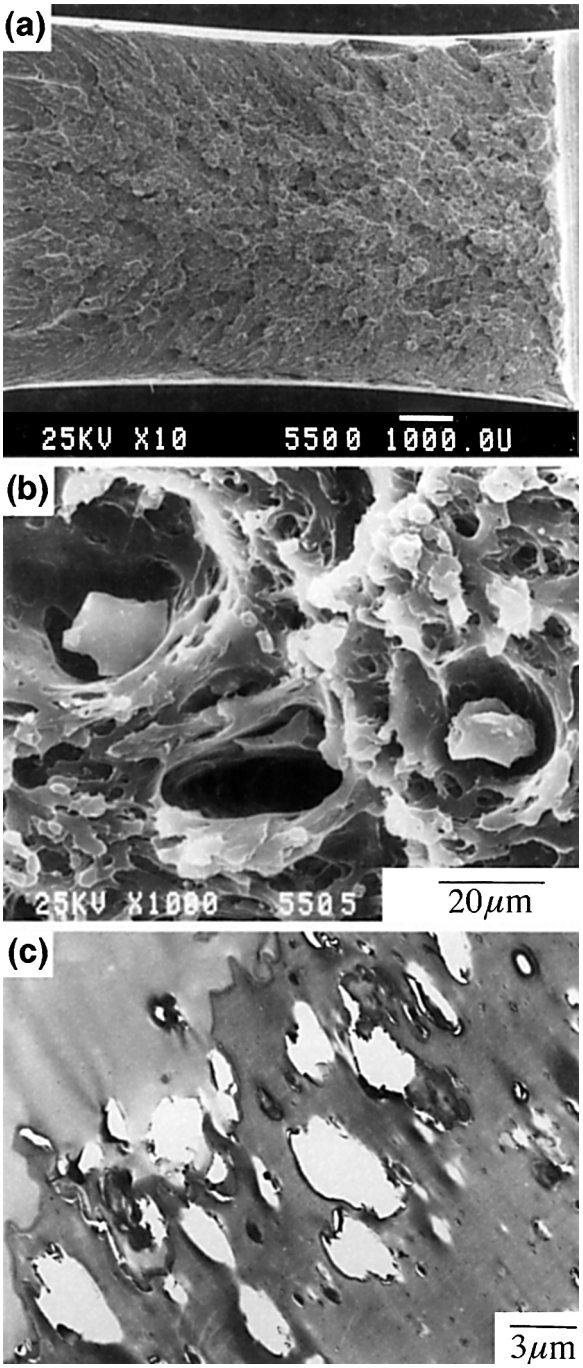


**Figure 17** Fracture surface of impacted PB-417: (a) low magnification of the entire surface (SEM); (b) a higher magnification of the fracture surface (SEM); (c) a longitudinal section through the damage zone; the fracture surface is visible in the upper left corner (TEM).

of the voids formed by cavitation of small particles could have initiated secondary cracks. An especially likely source of critical size voids was debonding of the very large particles. It was not surprising that the best impact was achieved in PC/PB blends when most of the rubber was dispersed as small particles, whereas when a large percentage of the rubber was present as large particles, the impact strength was very poor.

## CONCLUSIONS

A morphological study of PC blends with three butadiene-based impact modifiers has led to the following conclusions regarding the relationship of blend morphology to deformation mechanisms and Izod impact strength:

1. The Izod impact strength of PC/MBS blends is relatively insensitive to processing conditions. A little dispersive mixing together with some distributive mixing is sufficient to obtain good distribution of the presized 0.2 $\mu$m particles. Good impact of thick specimens is achieved when cavitation of the particles relieves the triaxiality and enables the matrix to fracture by the plane stress ductile tearing mode that is characteristic of thin PC. Coalescence of the cavitated particles that might lead to detrimental secondary crack initiation is not observed in PC/MBS blends.
2. The Izod impact strength of PC/SBS blends depends on the processing conditions since the rubber must be broken up into micron-sized particles. Overmixing of PC/SBS blends leads to a reduction in particle size that is responsible for a decrease in impact strength. Larger SBS particles ($> 1$ $\mu$m) are aggregates of small particles and cavitate at the weak internal boundaries. Small SBS particles (0.3–0.5 $\mu$m) without internal boundaries do not cavitate. Cavitation of the larger particles relieves the triaxiality, but coalescence of cavitated particles during ductile drawing of the matrix creates critical size voids; the resulting secondary cracks reduce the toughness of the blend.
3. In general, PB does not significantly enhance the impact strength of PC. Some blends exhibit enhanced impact strength; however, these are exceptions and it is difficult to control the processing to achieve reproducibility this property value. The particle-size distribution in PC/PB blends is very broad, with particle diameters ranging from 0.1 to 100 $\mu$m. The large particles serve as defects; fracture initiates from the large voids created when the particles debond from the matrix.

This research was generously supported by EniChem America Inc. and the National Science Foundation, I/UCRC Program (Grant EEC93-20055).

## REFERENCES

1. P. R. Soskey, R. P. Neu, H. H. Chin, S. Tuinstra, and K. A. Stromsland, *Polym. Process. Soc. Conf. Proc.*, **IX,** 155 (1993).
2. G. M. Swisber and R. D. Matbis, *Plast. Eng.*, **June,** 53 (1984).
3. D. W. Gilmore and M. J. Modic, *Plast. Eng.*, **April,** 51 (1989).
4. M. Nishimoto, H. Keskkula, and D. R. Paul, *Polymer,* **32,** 272 (1991).
5. R. J. Spontak, M. C. Williams, and C. N. Schooley, *J. Mater. Sci.*, **21,** 3173 (1986).
6. B. Fisa, B. D. Favis, and S. Bourgeois, *Polym. Eng. Sci.*, **30,** 1051 (1990).
7. M. P. Lee, A. Hiltner, and E. Baer, *Polymer,* **33,** 675 (1992).
8. S. Wu, *Polymer,* **26,** 1855 (1985).
9. A. J. Oshinski, H. Keskkula, and D. R. Paul, *Polymer,* **33,** 268, 284 (1992).
10. G. H. Michler, *Acta Polym.*, **44,** 113 (1993).
11. M. P. Lee, C. I. Kao, A. Hiltner, and E. Baer, *J. Mater. Sci.*, **28,** 1491 (1993).

*Received November 22, 1993*
*Accepted December 9, 1993*